B. TECH. PROJECT REPORT

On

Computational Micromechanical analysis of advanced Ceramic Matrix Composites (CMCs)

BY

Nilay Upadhyay
Anmol Kasera

DISCIPLINE OF MECHANICAL ENGINEERING
INDIAN INSTITUTE OF TECHNOLOGY INDORE
December 2019

Computational Micromechanical analysis of advanced Ceramic Matrix Composites (CMCs)

A PROJECT REPORT

Submitted in partial fulfillment of the requirements for the award of the degrees

of
BACHELOR OF TECHNOLOGY
in

MECHANICAL ENGINEERING

Submitted by:
Nilay Upadhyay
Anmol Kasera

Guided by:
Dr. Subbareddy Daggumati,
Assistant Professor

INDIAN INSTITUTE OF TECHNOLOGY INDORE
December 2019

Candidate's Declaration

We hereby declare that the project entitled **"Computational Micro-Mechanical analysis of advanced Ceramic Matrix Composites (CMCs)"** submitted in partial fulfillment for the award of the degree of Bachelor of Technology in 'Mechanical' completed under the supervision of **Dr. Subbareddy Daggumati, Assistant Professor, Department of Mechanical Engineering,** IIT Indore is an authentic work.

Further, we declare that we have not submitted this work for the award of any other degree elsewhere.

Signature and name of the student(s) with date

_____

CERTIFICATE by BTP Guide(s)

It is certified that the above statement made by the students is correct to the best of my/our knowledge.

Signature of BTP Guide(s) with dates and their designation

<u>Preface</u>

This report on "**Computational Micro-Mechanical analysis of advanced Ceramic Matrix Composites (CMCs)**" is prepared under the guidance of Dr. Subbareddy Daggumati.

The aim of this report was studying the effect of constituent level damage on the macroscopic stress-strain behavior of Ceramic Matrix Composite plies in longitudinal (Fiber) direction. The computational micromechanical analyses were performed on RVE models which contained finite thickness interface and interphase materials. There were two RVE models generated based on the unidirectional and 0/90 plies respectively. Different parameters were varied and their effect on the macroscopic stress-strain behavior of the composite was studied. Cohesive Zone Modeling (CZM) was used for the damage behavior of interface elements. In order to study the damage behavior of fiber, matrix and coating (interphase) elements, the Brittle Cracking model in Abaqus was used. A user material subroutine (VUMAT) was developed for the Brittle Cracking Model in Abaqus to visualize the damage initiation and failure of the material. We have tried to the best of our abilities and knowledge to explain the content in a lucid manner. We have also added 3-D models and figures to make it look more illustrative.

Nilay Upadhyay, Anmol Kasera
B.Tech. IV Year
Discipline of Mechanical Engineering
IIT Indore

<u>Acknowledgement</u>

Abstract

The current research work presents the computational micromechanical analysis of the room temperature fiber direction tensile failure behavior of a unidirectional (UD) and cross-ply (0/90) dimensional (3D) *Representative Volume Element (RVE)* and *Multi-fiber Multi-layer RVE (M^{2}RVE)* models are generated that are representative of the *lamina* and the *laminate* under investigation. The RVE and M^2 RVE models are generated by replicating the fiber distribution and the placement of the fibers observed in a microscopic image of an actual CMC laminate. The generated RVE models consist the discrete representation of individual constituent phases of the CMC such as fibers, interphase, matrix, and the fiber-interphase interface region. Under the applied external tensile load, the fiber-interphase interface interactions are modeled using the cohesive elements that follow the bi-linear traction separation law. The matrix, fiber, and the interphase material failure behavior is captured using the brittle cracking model. For the visualization of damage initiation and failure of the material, a user material subroutine (VUMAT) is developed incorporating the brittle cracking model in Abaqus. Using the proposed numerical methodology, a detailed local stress-strain and damage analysis lead to an observation that the "so-called" ductile stress-strain behavior (kink in the stress-strain curve) of the CMCs under uni-axial fiber direction tensile loads is mainly caused by the matrix damage initiation. Moreover, apart from the SiC material properties, it is also observed that the RVE size controls the strength and failure strain of the composite.

Keywords: Ceramic Matrix Composites (CMCs); Micromechanics; Finite Element Analysis (FEA); Cohesive Zone Modeling (CZM); Brittle cracking model, user subroutine (VUMAT).

Table of Contents

List of Figures

List of Tables

Chapter 1: Introduction

Ceramic Matrix Composites (CMCs) are attracting a lot of attention due to their specific applications in the high-temperature regions of gas turbines, aviation and aerospace industries. CMCs are lightweight and corrosion-resistant materials, which have higher specific stiffness and strength compared to the traditional metallic counterparts. Particularly, CMCs offer greater resistance to high-temperature environments ($>1250^\text{o}$C) when compared to metal and other engineering materials [1]. Moreover, utilization of the CMCs leads to the reduction in weight, fuel consumption as well as improvement in the thrust and the efficiency of the aero-engines [2]. Currently, CMCs are being utilized within the low in-service load regions (secondary structures) of the gas turbine components such as nozzles and combustor liners [3].

However, it is expected that with further improvements in the manufacturing process and the structural performance, these materials could be employed in the primary structures of the gas turbines such as turbine blades. In the aforementioned context, continuous fiber reinforced CMC material system fabricated using Silicon Carbide Fibers (SiC_f) embedded in Silicon Carbide (SiC) matrix exhibits high-temperature resistance as well as the high specific strength, rendering this particular material system suitable for gas turbine applications [3]. In a typical CMC material system, the SiC fibers are coated with a single or multiple layers of Boron Nitride (BN), which act as the so-called 'interphase' between the fibers and the matrix. The major functions of the interphase material in CMCs are: i) load transfer between fiber and matrix; ii) matrix crack deflection to increase the toughness of the composite; iii) providing environmental protection to the fibers.

From the structural response point of view, the individual fibers and matrix materials in SiCf/BN/SiC composites are brittle in nature. However, the CMC (SiCf/BN/SiC) composite material exhibits slight nonlinearly under the applied external tensile load [4]. It is a well understood fact that the aforementioned non-linear tensile response of CMCs serves as the means to redistribute stresses and eliminate stress concentration [5]. In addition, the

observed nonlinearity in the macroscopic stress-strain behavior of a composite ply is caused by the following microscopic phenomena occurring at the constituent level of the CMC: i) formation of matrix cracks; ii) crack propagation around the reinforcing fibers; iii) fiber-interphase interface debonding [6].

Since the environmental degradation of the fibers occurs through the already initiated matrix crack path [7], hence, here it should be emphasized that the *matrix cracking* is a critical damage mechanism for the service life of CMCs [8]. Therefore, in order to design efficient CMC structural components, it is of utmost importance to understand the initiation and interaction of damage mechanics between the different constituent materials, which leads to catastrophic failure of the composites [1].

In order to understand the influence of various microscale damage mechanisms on the macroscale stress-strain behavior of CMC (SiCf/BN/SiC) laminates, several researchers conducted detailed experimental studies at different length scales. Tracy et al. [9] conducted the tensile test on a CMC cross-ply laminate ([0/90/0/90]s) inside a Scanning Electron Microscope (SEM). The above-mentioned study concluded that the damage initiation occurs in the transverse (90°) plies that eventually lead to the composite laminate final failure. In order to study the detailed micro-scale matrix crack initiation and propagation mechanism in CMCs, Sevener et al. [8] conducted a tensile test on a CMC five-harness satin weave composite inside a Scanning Electron Microscope, combined with Digital Image Correlation (DIC).The aforementioned study concluded that the initiation of matrix cracks at microscale leads to a drop in the macroscopic stress. Dunn [4] conducted experimental studies to understand the fiber direction tensile failure behavior of unidirectional (0°) and cross-ply (0/90) CMC laminates (HiperComp®). The above-mentioned study concluded that the chosen fiber volume fraction shows a significant influence on the predicted strength and failure behavior of a laminate. As explained above, the non-linear macroscopic tensile stress-strain response of a CMC laminate loaded in the fiber direction is attributed to the microscale damage of the matrix material [10].

Finally, from the detailed experimental studies on CMC laminates, Mittal et al. [11]

2

concluded that the damage initiation and evolution in CMCs is related to architectural as well as microstructural details of the composite. From the above discussed experimental damage analysis, it is evident that the microscale damage initiation in the constituent CMC materials leads to the observed macroscopic non-linear stress-strain behavior.

In order to understand the effect of damage initiation in the constituent materials and its influence on the macroscopic stress-strain behavior, several researchers conducted detailed experimental studies at different length scales. However, a sequential and detailed damage analysis is missing at the microscopic length scale. This can be attributed to ease of conducting experiments as well as limitations in the experimental techniques that are used at lower length scales. In this regard, computational micromechanical modeling methodology provides a robust bottom-up (pyramidal) approach for understanding the influence of microscale parameters on the macroscopic stress-strain behavior [12] [13] [14] [15] [16] [17]. Moreover, the complex failure behavior of CMCs can be accurately captured through micromechanical RVE modeling, given that all individual micro-constituents such as fiber, matrix, interphase, and fiber-interphase interface are distinctly modeled and include in the RVE model [1] [18].

Within the framework of multiscale modeling, several researchers have worked on evaluating the mechanical behavior of CMCs using microscale models [18] [10] [19] [20] [21]. Chateau et al. [21] investigated the elastic behavior of high fiber volume fraction SiC$_f$/SiC composites by including the finite thickness pyrocarbon interphase in micromechanical models. Recent research work by Grujicic et al. [3] highlighted the effect of various microstructural parameters on the damage behavior of the gas-turbine CMCs using computational micromechanics. However, the aforementioned study assumed the perfect bonding between fiber and interphase rather than a weak cohesive bond. Even though several researchers conducted computational studies on CMCs, to the best of the authors' knowledge, a detailed micromechanical study regarding UD CMCs (SiC$_f$/BN/SiC) damage behavior under *longitudinal tensile loads* is missing in the literature. In addition, none of the aforementioned micromechanical studies attempted to predict the cross-ply (0/90) CMC laminate macroscopic stress-strain response using the computational

micromechanics approach.

In order to address the above discussed shortcomings related to the micromechanics of CMCs in the existing literature, the following objectives are laid out for current numerical study: i) the primary objective is to predict the macroscopic stress-strain behavior of a UD and cross-ply (0/90) CMC lamina and laminate, while understanding the effect of microscale parameters on the macroscopic stress-strain behavior; ii) the second objective is to study the effect of various parameters like _matrix fracture energy, matrix strength and RVE size_ on the predicted macroscopic stress-strain behavior of the composite. iii) The final objective of this project was to develop an appropriate damage model to incorporate the damage initiation and final failure of both uni-directional as well as 0/90 plies.

In order to realize the abovementioned objectives, a unidirectional CMC RVE and a multi-layer multi-fiber RVE (M^2RVE) models are generated to predict the macroscopic stress-strain response of a UD and a cross-ply laminate. Along with different constituent materials, the fibers distribution and the placement of the fibers in the RVE resembles the fiber architecture observed in a microscopic image of an actual CMC composite ply [4]. In order to capture the fiber-interphase interface interactions, the _Cohesive Zone Model (CZM)_ that follows the bi-linear traction separation law is used. _Following the previous research work of the authors [1], the interphase and the matrix surfaces in the RVE are tied together_. For modeling the failure behavior of various constituent materials such as _fiber, matrix, and interphase, brittle cracking model in Abaqus is used_. In order to study the effect of RVE size on the predicted numerical results, different RVE models are created with varying number of fibers and elements. The effect of matrix strength and fracture energy is depicted by performing micromechanical analysis on the same RVE and M^2RVE for different values. To study the damage initiation and failure of the matrix, fiber and interphase(coating) material in the composite, a user subroutine (VUMAT) was developed. The results through our methodology are the same as Abaqus in-built brittle cracking model results. _Using the above described computational micromechanical methodology, the obtained numerical results are thoroughly validated with the experimental results reported in [4]._

Chapter 2: Micromechanical modeling methodology

2.1 RVE FE models

In order to simulate the failure behavior of UD and cross-ply laminates, an RVE and M^2RVE models are generated based on the actual fiber distribution observed in the microscopic image of a CMC laminate [4]. The unidirectional CMC RVE model consists of 20 distinct SiC fibers having fiber diameters varying between 6 μm and 16 μm [4] (Fig 1a). In addition, for the coating material, a uniform thickness of 0.5 µm is assigned, which is equal to the average value of measured coating thickness from the microscopic image [4].
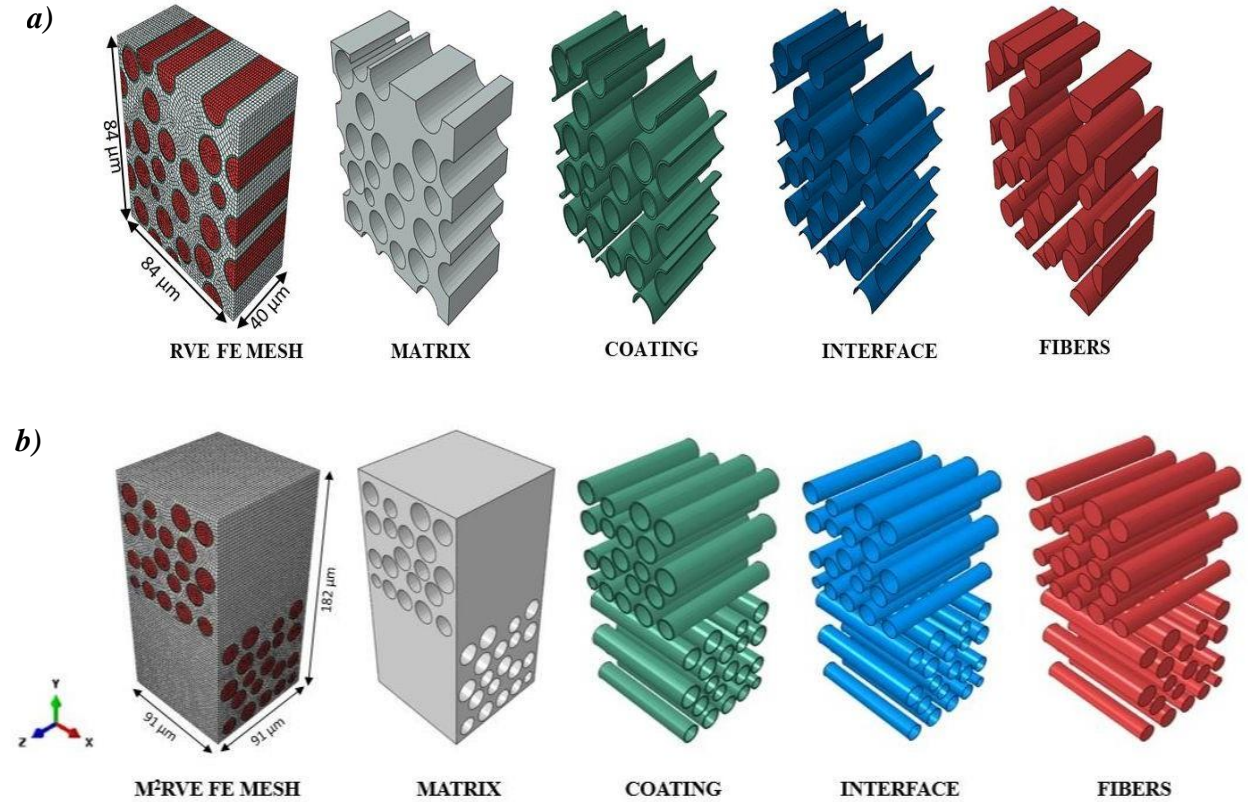
Figure 1 RVE models generation based on the microstructure: a) description of unidirectional CMC RVE with different constituent materials; b) M2RVE (cross-ply laminate) with different constituent materials.

Here, it should be highlighted that the variation in the fiber diameter, as well as the fiber placement in the RVE is replicated directly from the microscopic image. Followed by the

RVE model (Fig 1a) generation for lamina failure analysis, the M^2RVE model is generated for the laminate failure analysis by joining two cubic-shaped single layer multi-fibers RVEs with different fiber orientations (Fig 1b). Similar to the unidirectional CMC RVE, the fiber distribution of the M^2RVE is directly taken from the microscopic image of a CMC laminate. Here, it should be mentioned that the fiber volume fraction of both RVE and M^2RVE is maintained at 33%, which is equal to the fiber volume fraction of the CMC laminate [4].

After RVE and M^2RVE CAD models are generated, for the FE analysis these models are discretized using 3D solid hexagonal and wedge finite elements (i.e. C3D8R and C3D6R). Moreover, the *interface* between *fiber* and *interphase* is translated into FE mesh using 3D cohesive elements. The majority of the interface mesh consists of COH3D8 elements along with a few COH3D6 elements. Figures 1 (a, b) show the different constituents as well as the dimensions of the RVE and M^2RVE FE models respectively. Here it should be emphasized that the length and height of the RVE models are determined within the constraint of 33% fiber volumes fraction. From the micromechanical studies of polymer matrix composite, Totray et al.[22] concluded that the thickness of the RVE does not show any influence on the predicted stress-strain behavior. Hence, the chosen thickness for the current RVE and M^2 RVE models are based on the lower computational cost as well as the optimum aspect ratio for the FE mesh. Finally, in order to study the effect of the number of fibers in the RVE on the predicted average stress-strain behavior, a detailed parametric study is conducted and the results are presented in the following section.

From the perspective of boundary conditions, the Periodic Boundary Conditions (PBCs) are most suitable for micromechanical simulations. As stated by Garoz et al.[23], imposing PBCs makes it possible to "*represent an infinitely large system using a small domain (RVE) replicated in three spatial directions*". Hence, PBCs were imposed on the faces, edges, and vertices of both RVE and M^2RVE models as specified in [1]. Here it should be highlighted that RVE models generation process, as well as PBCs application to the RVE is automated with the python and MATLAB scripts respectively.

2.2 Fiber-interphase *interface* damage modeling (*cohesive zone modeling*)

The interface interactions between fiber and interphase materials are captured using the Cohesive Zone Modeling (CZM) approach. The constitutive response of the interface cohesive elements is assumed to be governed by a bi-linear traction-separation law, which relates the separation across the interface with the traction vector acting upon it (Fig 2). As shown in Fig 2, the overall mechanical behavior of the interface can be distinguished as two separate regions: i) linear elastic region up to the point of *interface element damage initiation*; ii) linear softening behavior from *damage initiation* to the point of *complete element failure*. The linear elastic region is prescribed by a fictitious stiffness value 'K' which ensures that the displacement continuity exists across the fiber-interphase interface region. The constitutive equation for the linear elastic behavior of the aforesaid traction separation law is defined through the following equation [24].
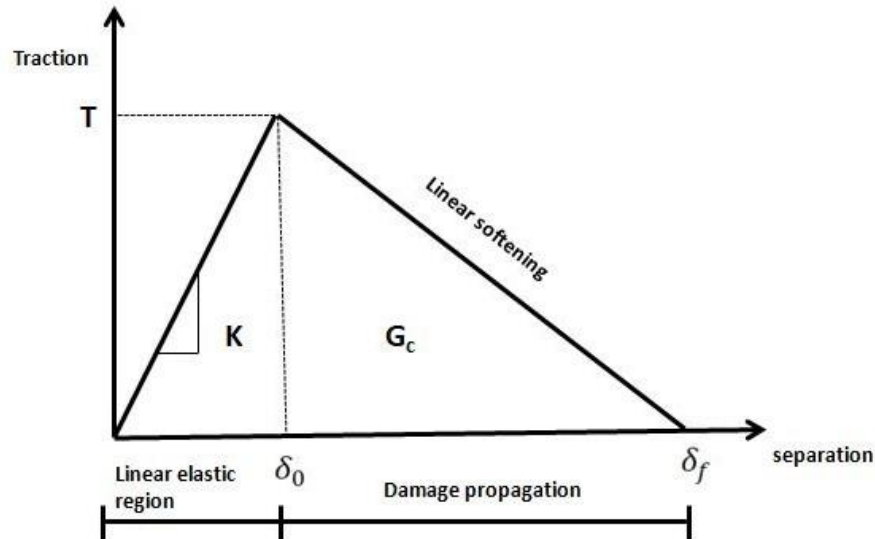
Figure 2 Bi-linear traction separation law used for the cohesive elements

$$T^L = \begin{bmatrix} T_s \\ T_t \\ T_n \end{bmatrix} = \begin{bmatrix} K & 0 & 0 \\ 0 & K & 0 \\ 0 & 0 & K \end{bmatrix} \begin{bmatrix} \delta_s \\ \delta_t \\ \delta_n \end{bmatrix} \tag{1}$$

In the above equation, Tn, Ts, and Tt are the normal (Mode I) and shear (Mode II & Mode III) stresses at the interface, while the corresponding displacements are denoted by δn, δs, and δt respectively. In addition, TL denotes the stresses corresponding to the linear elastic region. As soon as the interface cohesive element stress reaches a threshold value, the damage initiation is identified using the following mixed-mode quadratic nominal stress criterion [18]:

$$\left\{\frac{\langle T_n \rangle}{T_n^0}\right\}^2 + \left\{\frac{T_s}{T_s^0}\right\}^2 + \left\{\frac{T_t}{T_t^0}\right\}^2 = 1 \tag{2}$$

In the above equation, $\langle \cdot \rangle$ indicates the Macaulay bracket, which is defined as $\langle \cdot \rangle = \frac{1}{2}(\cdot + |\cdot|)$. Here, it should be noted that the utilization of the Macaulay bracket implies that compressive normal loading does not cause the interface damage initiation. Moreover, T_n, T_s, and T_t are the normal (Mode I), shear (Mode II) and tangential stresses (Mode II) at the interface respectively. In addition,T_n^0, T_s^0, and T_t^0 are the corresponding individual strengths of the interface n T0s T0t in that particular mode. The linear softening behavior of the interface is defined through the utilization of a mode I based damage evolution law. Once the interface damage initiates, the interface stress reduces linearly with respect to displacement depending upon the following damage variable 'D' [24].

$$D = \frac{\delta_n^f(\delta_n^{max}-\delta_n^0)}{\delta_n^{max}(\delta_n^f-\delta_n^0)} \tag{3}$$

In equation 3, δ_n^{max} is the maximum normal mode separation attained during loading history; δ_n^0 is the effective normal mode displacement at the damage initiation (D = 0) and δ_n^f is the displacement at complete failure (D = 1). The critical fracture energy G_n^c of the interface elements is defined as the area under the traction-separation curve. The normal mode displacement for the interface is computed using the following set of expressions.

$$\delta_n^f = \frac{2G_n^c}{T_n^0} \tag{4}$$

Where, $T_n^0 = K\delta_n^0$

Finally, the damage evolution is described by the following equation [24].

$$\tau = \begin{cases} T^L & ; \delta_n^{max} \leq \delta^0 \\ (1-D)K\delta_i, i = n, s, t; \delta_n^{max} > \delta^0 \end{cases} \quad (5)$$

The material properties utilized for interface damage initiation as well as damage evolution are listed in Table 1 and Table 2.

Table 1: Elastic material properties for fibers, matrix, and coating materials

Material	Young's Modulus (GPa)			Poisson's Ratio			Shear Modulus (GPa)		
	E_{11}	E_{22}	E_{33}	v_{12}	v_{13}	v_{23}	G12	G13	G23
SiC Fiber	370 [3]	200 [3]	200 [3]	0.25 [3]	0.25 [3]	0.22 [3]	80 [3]	80 [3]	82 [3]
SiC Matrix	350 [29]	350 [29]	350 [29]	0.17 [29]	0.17 [29]	0.17 [29]	-	-	-
BN Coating	10 [18]	10 [18]	10 [18]	0.05 [18]	0.05 [18]	0.05 [18]	-	-	-

Table 2: Strength properties for fibers, matrix, and coating materials

Material	Strength	Fracture Energy (J/m^2)
SiC Fiber	2600 [18]	83±18 [30]
SiC Matrix	800 [18]	83±18 [30]
BN Coating	75 [18]	5 [18]
Interface	75 [1]	5 [1]

2.3 Fiber, matrix and interphase materials damage modeling *(brittle fracture criteria)*

In order to model the fracture behavior of the fibers, matrix and interphase materials, Abaqus®
built-in brittle cracking model is utilized. The aforementioned brittle cracking model is based on
smeared crack assumptions to represent the brittle failure behavior of a material. Under the
smeared crack modeling approach, instead of modeling a discrete crack, the effect of a crack is
directly included in the constitutive response of the material. Thus, contrary to the traditional
fracture mechanics approach, there is no geometrical *crack-like* discontinuity present in the
current material model. As soon as the local stress at any integration point of an element exceeds
the tensile strength of the material, the maximum principal tensile stress criterion is used to
initiate the damage. The direction of damage propagation is assumed to be aligned normal to the
principal plane corresponding to maximum principal tensile stress. During the crack propagation,
the total incremental strain ($d\epsilon$) is decomposed into elastic ($d\epsilon^{el}$) and cracking strain ($d\epsilon^{ck}$) as
per the following equation [24].

$$d\epsilon = d\epsilon^{el} + d\epsilon^{ck} \tag{6}$$

The stresses across the crack are computed with respect to a local coordinate system which is
aligned to the crack direction (Fig 3). Consequently, the strain in global (ϵ) and the local
coordinate system (e) is described through the following set of equations.

$$\epsilon = [\epsilon_{11} \quad \epsilon_{22} \quad \epsilon_{33} \quad \gamma_{12} \quad \gamma_{13} \quad \gamma_{23}]^{\mathrm{T}} \tag{7}$$

$$e = [e_{nn}^{ck} \quad e_{tt}^{ck} \quad e_{ss}^{ck} \quad g_{nt}^{ck} \quad g_{ns}^{ck} \quad g_{ts}^{ck}]^{\mathrm{T}} \tag{8}$$
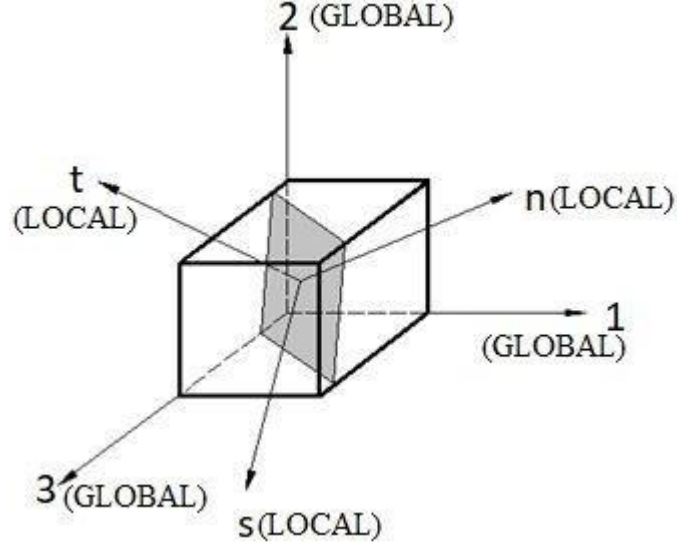
Figure 3 Description of the global and local coordinate systems for the brittle cracking model [24].

In the above equation, $e_{nn}^{ck}, e_{tt}^{ck},$ and e_{ss}^{ck} are the normal strains whereas $g_{nt}^{ck}, g_{ns}^{ck},$ and g_{ts}^{ck} correspond to shear strain at crack location. The abovementioned strain-transformation can be expressed in the matrix form as follows:

$$\epsilon = Te \tag{9}$$

In Eqn 9, T is the transformation matrix constructed from the direction cosines of the local Cartesian system. Similar to the strain, the stress quantities in global (σ) and local (t) coordinate systems are given by the following set of expressions.

$$\sigma = [\sigma_{11} \quad \sigma_{22} \quad \sigma_{33} \quad \sigma_{12} \quad \sigma_{13} \quad \sigma_{23}]^T \tag{10}$$

$$t = [t_{nn} \quad t_{tt} \quad t_{ss} \quad t_{nt} \quad t_{ns} \quad t_{ts}]^T \tag{11}$$

$$t = T^T \sigma \tag{12}$$

Using the strain decomposition and the elastic stress-strain relations, the increment in the stress can be defined as [25].

$$d\sigma = D^{el}(d\epsilon - Tde^{ck}) \qquad (13)$$

In the above equation, D^{el} is the isotropic linear elasticity matrix. The relation between the incremental local stresses (dt) and the incremental local cracking strains (de^{ck}) at the crack interfaces is given by the following expression [24][25].

$$dt = D^{ck}de^{ck} \qquad (14)$$

Where, $D^{ck} = \text{diag}\,[D^I_{nn}, D^I_{tt}, D^I_{ss}, D^{II}_{nt}, D^{II}_{ts}, D^{II}_{ns}]$

In the above equation, D^{ck} is the diagonal cracking matrix that relates the post-cracking stress-strain behaviour of the material. Combining equations 12, 13 and 14 results in the following incremental stress-strain equation during the crack propagation [24][25].

$$d\sigma = [D^{el} - D^{el}T(D^{ck} + T^TD^{el}T)^{-1}\,T^TD^{el}]d\epsilon \qquad (15)$$

As shown in Eqn 14, the diagonal matrix D^{ck} incorporates individual mode I based as well as mode-II dependent damaged stiffness values. Hence, it is clear that the post cracking stress-strain behavior depends on both Mode-I as well as Mode-II fracture. Consequently, the mode-I based post-cracking behavior is discussed first, and the details regarding mode-II based crack evolution are presented in the latter part of the current section.

The mode-I based crack evolution (tension softening model) is defined on the basis of the fracture energy concept of Hillerborg et al. [26]. In this approach, the post cracking behavior of the material is described through a gradually decreasing stress-displacement relation [27], which is defined by the following expression [24].

$$G^I_f = \int \sigma^I_t \, du_n \qquad (16)$$

In the above equation, G^I_f is the fracture energy required to generate a unit area of the crack surface. While u_n corresponds to the normal opening displacement. The normal crack opening

(u_n^{ck}) displacement is computed by multiplying the cracking strain in the normal direction (u_n^{ck}) with the characteristic length h associated with the material point (Eqn 17).

$$u_n^{ck} = e^{ck}h \tag{17}$$

Utilization of the characteristic length based approach alleviates the FE mesh size dependency associated with the material softening behavior due to damage. Here, it should be mentioned that the characteristic length (h) depends on the element geometry and formulation. For solid elements, the characteristic length is equal to the cubic root of the element volume [24]. Finally, under the assumption of linear strength degradation, the post-cracking stress-fracture energy relation is described in terms of the following expression [24].

$$\sigma_{bt}^I = \frac{2G_f^I}{u_n^f} \tag{18}$$

In the above equation, σ_{bt}^I is the tensile strength of the brittle material and u_n^f corresponds to the normal displacement of the crack at which complete loss of the material strength takes place. The individual mode I based damaged stiffness values $(D_{nn}^I, D_{tt}^I, D_{ss}^I)$ can be described by the following expression [25].

$$D_{ii}^I = \frac{\sigma_{bt}^I{}^2 h}{2G_f^I}; i = n, s, t \tag{19}$$

The mode-II based crack evolution is described by a shear retention model [24]. The aforementioned mode-II based damaged stiffness values $(D_{nt}^{II}, D_{ts}^{II}, D_{ns}^{II})$ can be written in a concise form as D_{jj}^{II}. The shear stress across the crack (t_{ij}) is defined as a function of local shear strain g_{ij}^{ck} [24].

$$t_{ij} = D_{jj}^{II}g_{ij}^{ck} ; [i = n, s, t ; j = n, s, t] \tag{20}$$

Where, $D_{jj}^{II} = \alpha(e_{ii}^{ck}e_{jj}^{ck})G$

As shown from the above equation (Eqn 20), the post cracking mode II based shear stiffness (D_{jj}^{II}) depends on crack opening strains (i.e e_{nn}^{ck} and e_{tt}^{ck}). G is the shear modulus prior to damage initiation in the material and $\alpha\left(e_{ii}^{ck}e_{jj}^{ck}\right)$ is the power-law function proposed by Rots et.al. [28]. Moreover, $\alpha\left(e_{ii}^{ck}e_{jj}^{ck}\right)$ is always defined for single individual mode dependent crack opening strain (i.e. i = j) and is given by the following equation [24] [28].

$$\alpha\left(e_{ii}^{ck}\right) = \frac{\left(1-\dfrac{e_{ii}^{ck}}{max_{over\,history}^{e_{ii}^{ck}}}\right)^{p}}{1-\left(1-\dfrac{e_{ii}^{ck}}{max_{over\,history}^{e_{ii}^{ck}}}\right)^{p}} \tag{21}$$

In the above equation, the term $max_{over\,history}^{e_{ii}^{ck}}$ denotes the maximum value of cracking strain attained during loading history at the corresponding material point. Here, it should be noted that the Eqn. 20 is utilized when the crack opens in only one direction, i.e. either normal or shear direction. However, if the crack opens in two different directions (*n and t/s*) then the following expression is utilized for the computation of D_{ij}^{II}.

$$D_{ij}^{II} = \frac{\alpha\left(e_{ii}^{ck}\right)*\alpha\left(e_{jj}^{ck}\right)G}{\alpha\left(e_{ii}^{ck}\right)+\alpha\left(e_{jj}^{ck}\right)} \tag{22}$$

We have developed a user material subroutine (VUMAT) in Abaqus to include the aforementioned material damage model. The in-built Abaqus brittle cracking model fails to provide a suitable visualization of damage initiation and final failure of the material. Thus, for the purpose of studying the damage initiation and its subsequent propagation in the fiber, matrix and interphase materials, we programmed a subroutine based on the brittle cracking model in Abaqus. This VUMAT code included several State Dependent Variables (SDVs) in the output file to obtain the visualization of the above discussed damage evolution.

2.3.1: Flow chart for the VUMAT code developed for Brittle Cracking.

Flow chart (left side):

Start → Load Increment → Calculate Stresses $d\sigma = D^{el}\,d\varepsilon$ → Damage Initiated? (if $\sigma_{mp} > \sigma_t$)

- No → back to Calculate Stresses
- Yes → Calculate D^f (Damaged stiffness matrix) → Calculate Stresses $d\sigma = D^f\,d\varepsilon$ → Stress New=0?
  - No → back to Load Increment
  - Yes → Stop

Elastic stiffness matrix:

$$\begin{bmatrix} d\sigma_{xx} \\ d\sigma_{yy} \\ d\sigma_{zz} \\ d\sigma_{xy} \\ d\sigma_{xz} \\ d\sigma_{yz} \end{bmatrix} = \begin{bmatrix} \lambda+2\mu & \lambda & \lambda & 0 & 0 & 0 \\ \lambda & \lambda+2\mu & \lambda & 0 & 0 & 0 \\ \lambda & \lambda & \lambda+2\mu & 0 & 0 & 0 \\ 0 & 0 & 0 & 2\mu & 0 & 0 \\ 0 & 0 & 0 & 0 & 2\mu & 0 \\ 0 & 0 & 0 & 0 & 0 & 2\mu \end{bmatrix} \begin{bmatrix} d\varepsilon_{xx} \\ d\varepsilon_{yy} \\ d\varepsilon_{zz} \\ d\varepsilon_{xy} \\ d\varepsilon_{xz} \\ d\varepsilon_{yz} \end{bmatrix}$$

$2\mu = E/(1+v), \quad \lambda = 2\mu v/(1-2v)$

Transformation Matrix, T

$$\begin{bmatrix} l_1^2 & m_1^2 & n_1^2 & 2l_1m_1 & 2m_1n_1 & 2n_1l_1 \\ l_2^2 & m_2^2 & n_2^2 & 2l_2m_2 & 2m_2n_2 & 2n_2l_2 \\ l_3^2 & m_3^2 & n_3^2 & 2l_3m_3 & 2m_3n_3 & 2n_3l_3 \\ l_1l_2 & m_1m_2 & n_1n_2 & l_1m_2+m_1l_2 & m_1n_2+n_1m_2 & n_1l_2+l_1n_2 \\ l_2l_3 & m_2m_3 & n_2n_3 & l_2m_3+m_2l_3 & m_2n_3+n_2m_3 & n_2l_3+l_2n_3 \\ l_3l_1 & m_3m_1 & n_3n_1 & l_3m_1+m_3l_1 & m_3n_1+n_3m_1 & n_3l_1+l_3n_1 \end{bmatrix}$$

Where l, m and n are direction cosines for the three eigen vectors.

Computation of D^f

- Cracking strain, $e^{ck} = T\,d\varepsilon$

$$\alpha(e_{ii}^{ck}) = \frac{\left(1 - \dfrac{e_{ii}^{ck}}{\max_{\text{over history}}(e_{ii}^{ck})}\right)^p}{1 - \left(1 - \dfrac{e_{ii}^{ck}}{\max_{\text{over history}}(e_{ii}^{ck})}\right)^p}$$
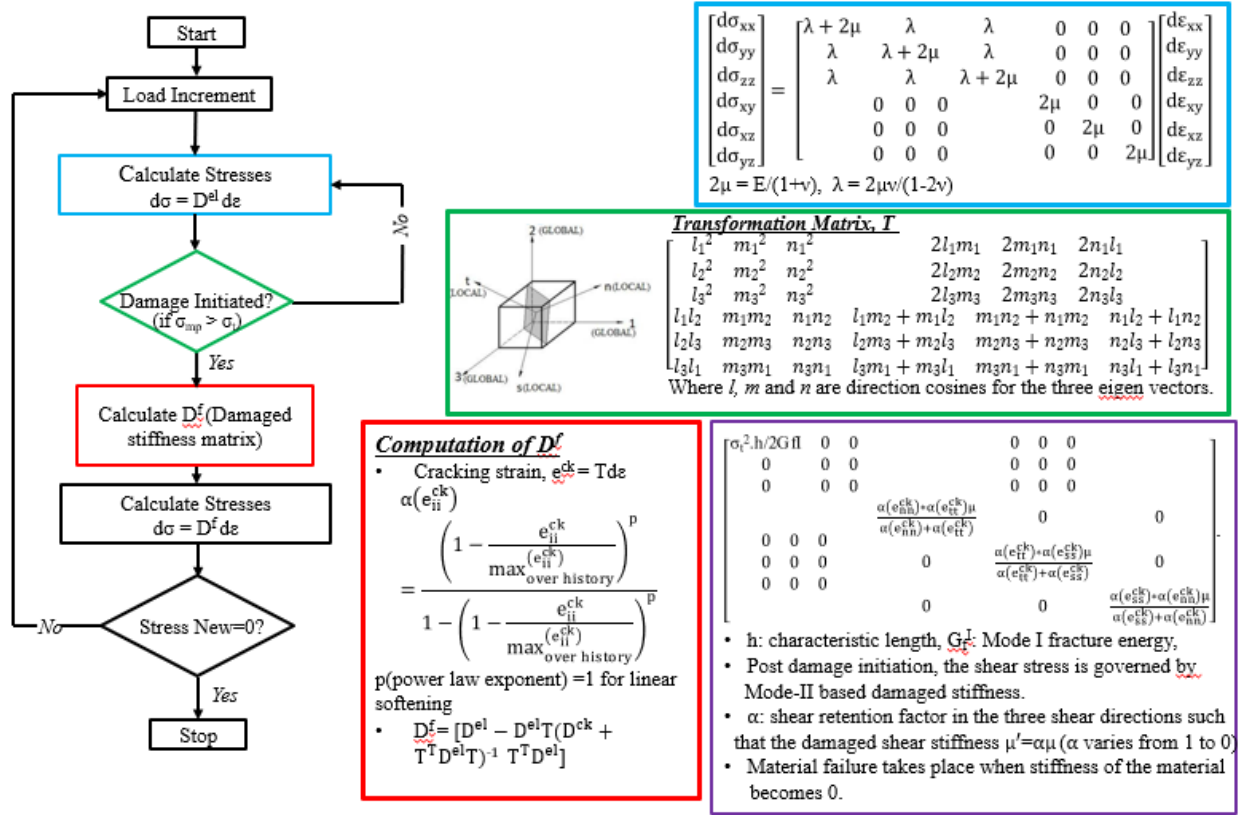
p(power law exponent) =1 for linear softening

- $D^f = [D^{el} - D^{el}T(D^{ck} + T^TD^{el}T)^{-1} T^TD^{el}]$

Cracking stiffness matrix D^{ck}:

$$\begin{bmatrix} \sigma_t^2 \cdot h/2G_f^I & 0 & 0 & 0 & 0 & 0 \\ 0 & 0 & 0 & 0 & 0 & 0 \\ 0 & 0 & 0 & 0 & 0 & 0 \\ 0 & 0 & 0 & \frac{\alpha(e_{nn}^{ck})+\alpha(e_{tt}^{ck})\mu}{\alpha(e_{nn}^{ck})+\alpha(e_{tt}^{ck})} & 0 & 0 \\ 0 & 0 & 0 & 0 & \frac{\alpha(e_{tt}^{ck})+\alpha(e_{ss}^{ck})\mu}{\alpha(e_{tt}^{ck})+\alpha(e_{ss}^{ck})} & 0 \\ 0 & 0 & 0 & 0 & 0 & \frac{\alpha(e_{ss}^{ck})+\alpha(e_{nn}^{ck})\mu}{\alpha(e_{ss}^{ck})+\alpha(e_{nn}^{ck})} \end{bmatrix}$$

- h: characteristic length, G_f^I: Mode I fracture energy,
- Post damage initiation, the shear stress is governed by Mode-II based damaged stiffness.
- α: shear retention factor in the three shear directions such that the damaged shear stiffness $\mu' = \alpha\mu$ (α varies from 1 to 0)
- Material failure takes place when stiffness of the material becomes 0.

On the application of load before damage initiation, the stresses calculation takes through the elastic stiffness matrix. The damage initiation takes place when the max principal stress in the material exceeds the tensile strength of the material. The principal stresses are calculated in the subroutine by the Abaqus in-built subroutine VUSPRIND. On passing the stress matrix to the subroutine, it returns the maximum principal stress along with the direction cosines of the three eigen vectors. Once the damage initiates in the material, these returned direction cosines are then used to calculate the transformation matrix T. The subroutine then calculates the damaged stiffness matrix D^f which is calculated by the Equation (15) where D^{ck} is the cracking stiffness matrix which contains terms for both Mode I and Mode II softening. For Mode I softening, Mode I fracture energy is used and for Mode II softening, the shear retention terms are incorporated. The post damage initiation shear stiffness (μ') depends on the shear retention factor (α) such that

$$\mu' = \alpha\mu \qquad (23)$$

where μ is the initial shear modulus. The material point is killed when the stiffness of the material becomes zero and it cannot sustain any further loads and the subroutine stops.

15

Chapter 3: Results and discussion

3.1 RVE under longitudinal tension – *UD ply stress-strain and damage analysis*

Using the above discussed numerical methodology, for a detailed analysis of the local stress-strain and damage profiles, *initial FE simulation was accomplished with an RVE that consists of a single SiC fiber embedded in the SiC matrix*. For simulating the matrix and the coating elastic stress-strain behavior, isotropic materials properties listed in Table 1 are used. However, the elastic stress-strain behavior of the fiber is simulated by assigning transversely isotropic material properties (Table 1) reported by Evans et al. [29]. Moreover, in order to ensure continuity of load transfer between *fiber-interphase* interface regions, an initial stiffness of 1E+7 MPa/mm is assigned to the interface elements. Finally, for simulating the constituent materials damage initiation and progression the strength and fracture energy values listed in Table 2 are used.

Fig 4a compares the average stress-strain curve obtained from the single fiber RVE FE simulations to the experimental UD laminate stress-strain curve [4]. As shown in Fig 4a, until the applied average fiber direction tensile stress reaches approximately 650 MPa, almost a linear stress-strain behavior is observed. As soon as the average tensile stress reaches 653 MPa, matrix damage initiates (Fig 4b) and leads to the kink in the average stress-strain response. Followed by the matrix damage, fiber-interphase *interface elements* damage is detected at around 710 MPa average tensile stress (Fig 4c).
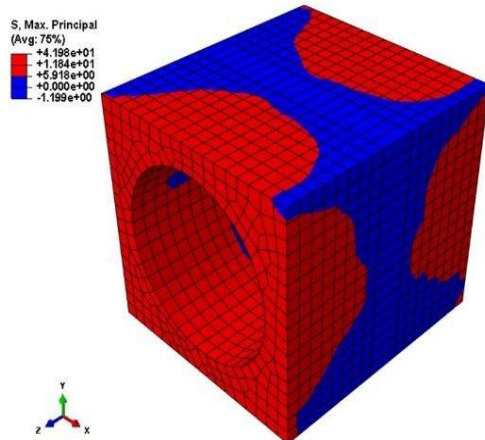
a) RVE under Longitudinal Tension
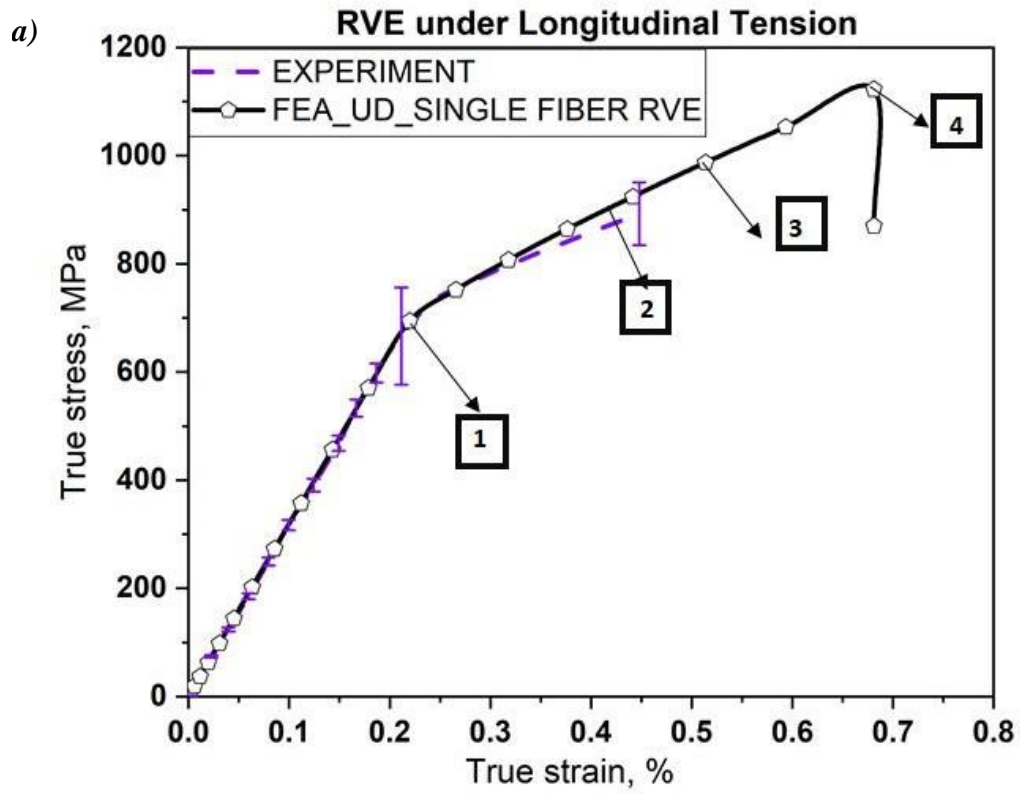
1. Matrix crack
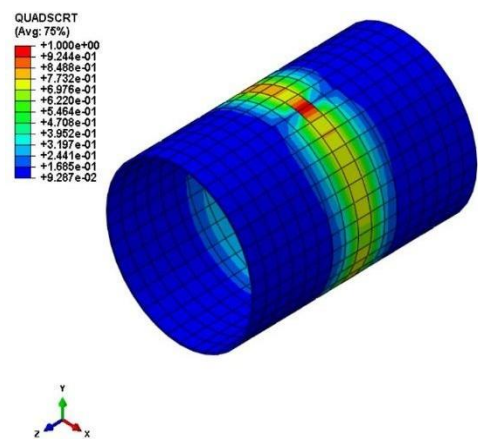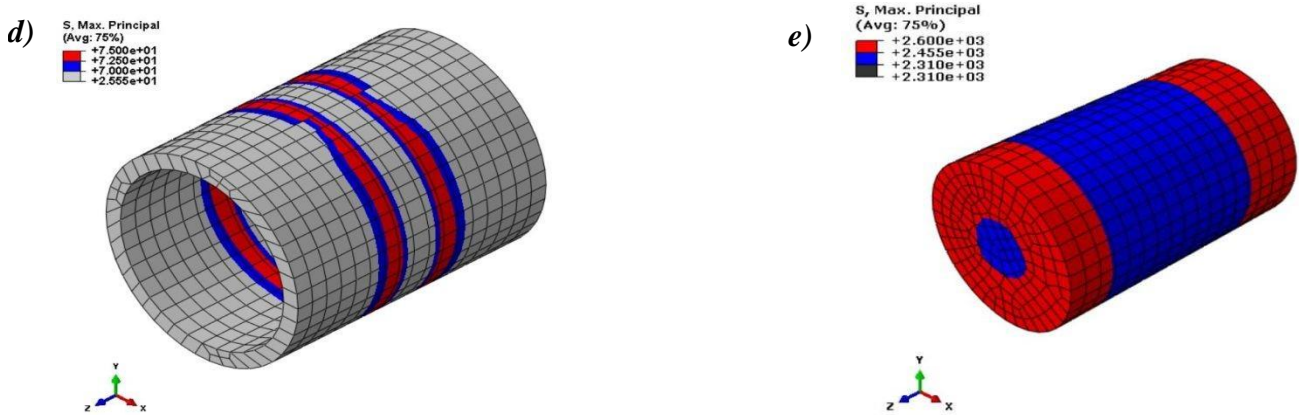2. Interface damage
3. Interphase damage
4. Fiber failure

b)

c)

17

Figure 4 Single fiber RVE under fiber direction tensile load (UD): a) comparison between experimental [4] and numerical stress-strain curve; b) matrix damage; c) interface damage; d) coating (interphase) damage; e) fiber failure.

Later, interphase (BN) damage occurs at 788 MPa tensile stress. Finally, at around 1130 MPa fiber failure is detected, which leads to the complete failure of the RVE. From Fig 4a one can observe that, after matrix crack initiation, the predicted average stress-strain curve deviates from the experimental stress-strain curve. The discrepancy between the experimental and numerical stress-strain curves can be attributed to the following factor. For the current FE analysis, single fiber RVE is used to understand the sequence of damage events that are occurring in various constituent materials of the RVE. However, by considering the single fiber RVE, the effect of neighbouring fibers stress concentration on the predicted damage behavior is neglected. Hence, the following section provides a detailed study on the effect of RVE size on the predicted average stress-strain response.

3.1.1 RVE under longitudinal tension – *Effect of RVE size*

Fig 5a compares the predicted average stress-strain curves obtained using RVEs with the varying number of fibers (10, 15, and 20). As explained above, all these RVE models are constructed based on the fiber placement observed from the microscopic image of an actual UD CMC ply. As shown in Fig 5a, *RVE size does not show any influence in the linear elastic region of the stress-strain curve*. However, as anticipated, local compaction of the fibers enhance the matrix

stress concentration and propagate the damage much earlier compared to the single fiber RVE. Hence, after the matrix damage initiation, the predicted stress-strain curve using multiple fibers RVE deviates substantially from the single fiber RVE.

Moreover, the average stress-strain curve predicted using 15 and 20 fibers RVE correlates very well with the experimental stress-strain curve. The observed sequence of damage events in multiple fiber RVE's (Fig 5b-e) is similar to that of single fiber RVE. *From the computational studies conducted using different RVEs with the varying number of fibers indicate that an RVE should contain at least 15 randomly distributed fibers so that the predicted average stress-strain behavior using this volume element is independent of its size and position with the lamina.*

a)
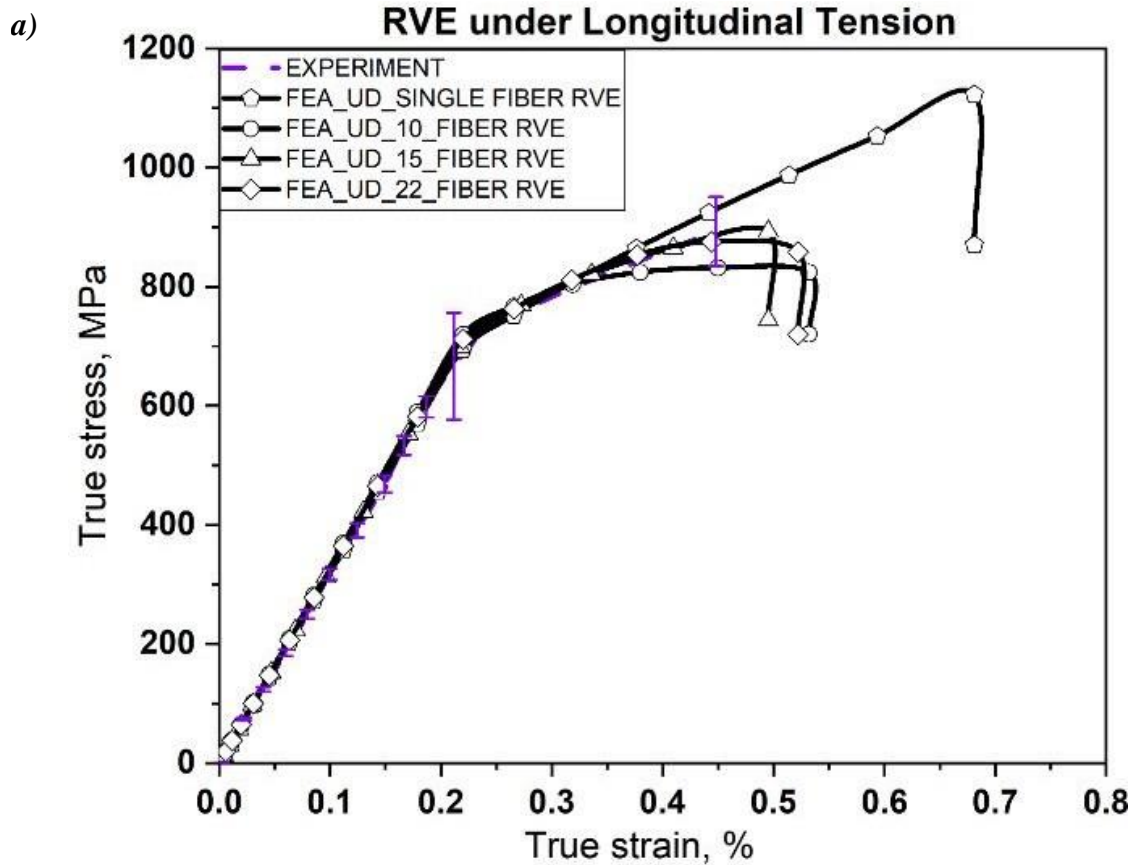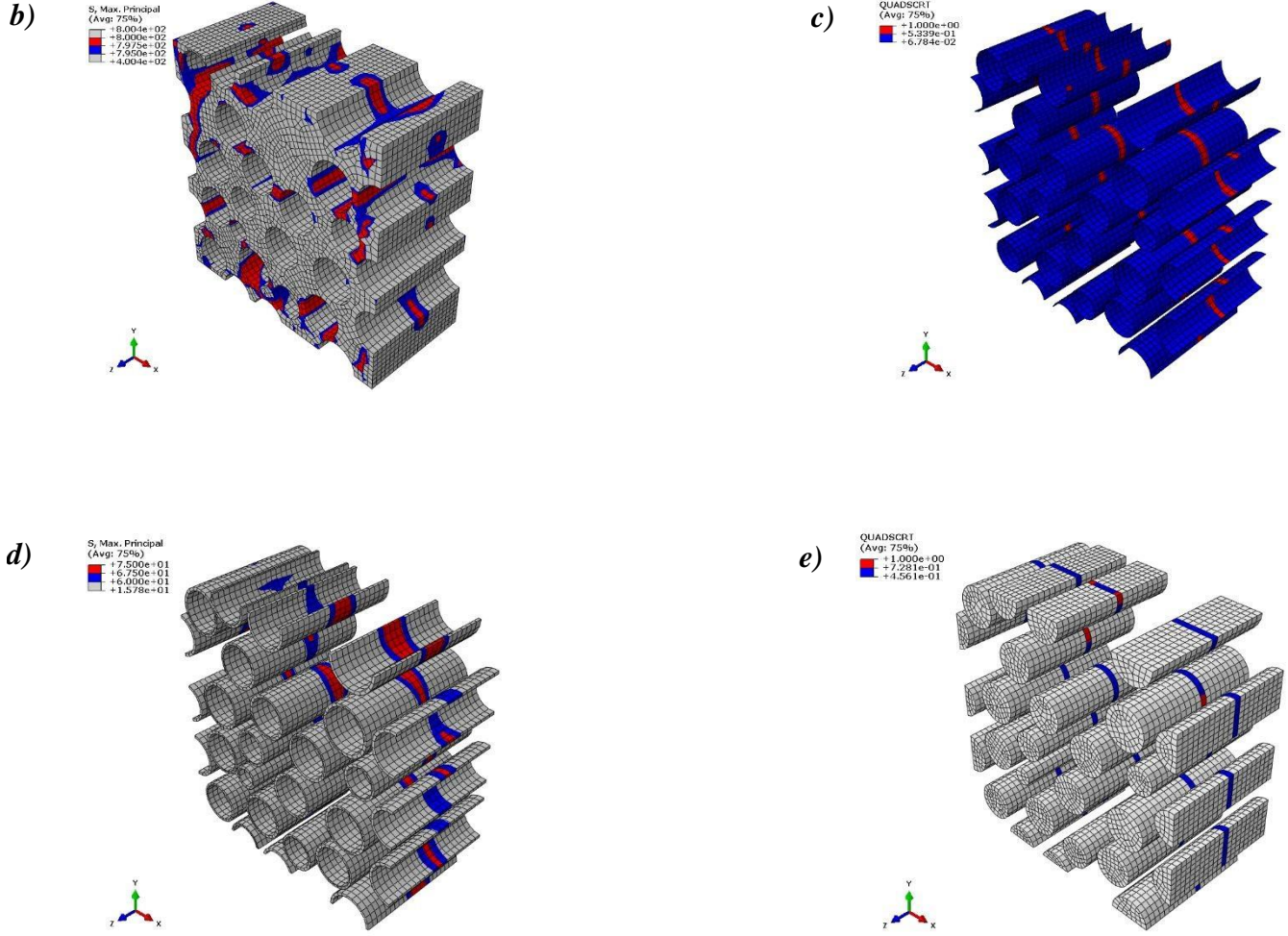
Figure 5 Effect of RVE size on the stress-strain and damage behavior: a) comparison between experimental [4] and numerical stress-strain curve; b) matrix damage; c) interface damage; d) coating (interphase) damage; e) fiber failure.

3.1.2 RVE under longitudinal tension – *Effect of matrix material properties*

As discussed above, once the *matrix damage initiates* the slope of the stress-strain curve changes considerably (Fig 5a). Hence, the effect of matrix material properties on the predicted stress-strain behavior of the RVE is studied in this section. For the current study, the matrix (SiC) tensile strength is varied from 400-1000 MPa [18] while keeping the fracture energy constant at 83 J/m2. As shown in Fig 6a, the chosen matrix tensile strength strongly influences the predicted average stress-strain behavior. In order to study the effect of matrix fracture energy on the

predicted stress-strain behavior, the matrix strength value is kept constant at 800 MPa and the fracture energy value is varied from 65-101 J/m2 [30]. As shown in Fig 6b, the slope of the predicted stress-strain curve in the non-linear region is strongly influenced by the chosen fracture energy. *From the current studies, we can conclude that the linear elastic stress-strain limit of the RVE is controlled by the matrix tensile strength. Whereas the average stress-strain behavior in the non-linear region is controlled by the matrix fracture energy.*
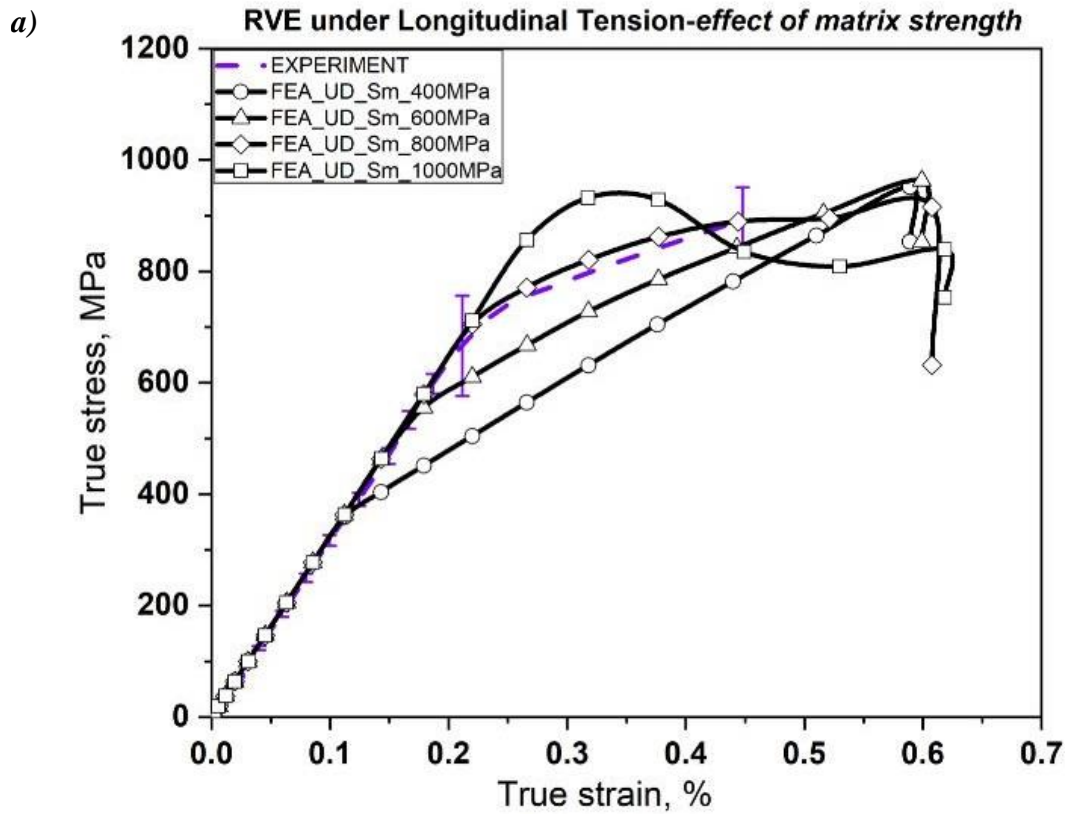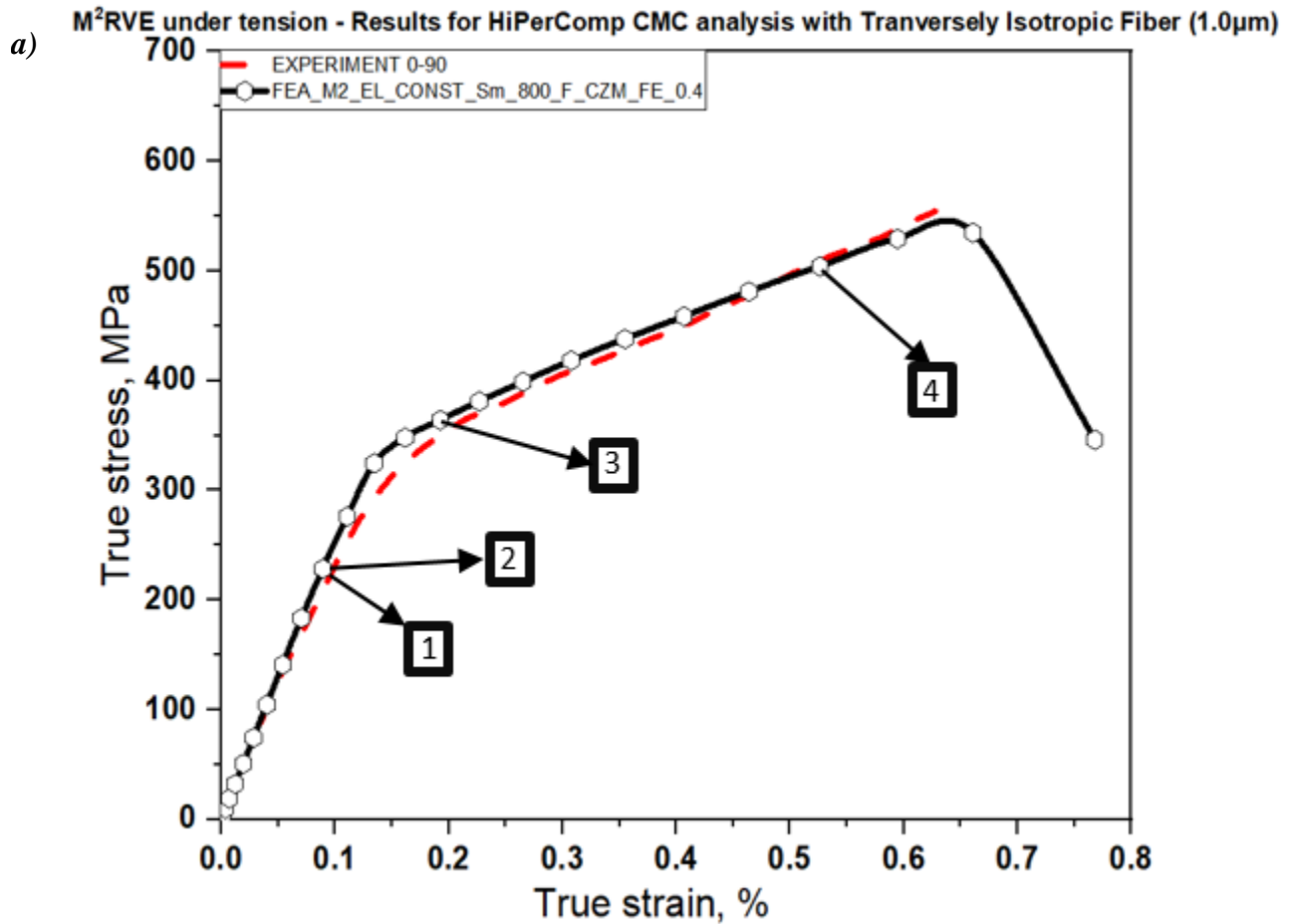
b)
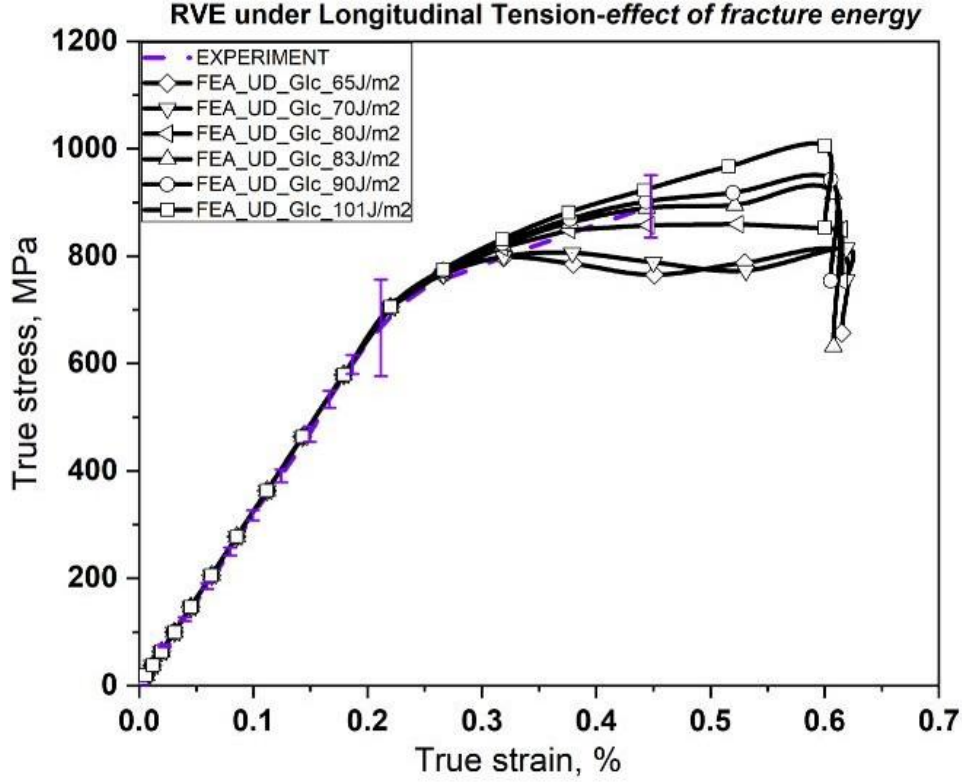
Figure 6 Effect of matrix material properties on the predicted stress-strain behavior: a) influence of the matrix (SiC) tensile strength; b) influence of matrix fracture energy.

## 3.2 M²RVE under longitudinal tension – *Cross-ply laminate stress-strain and damage analysis*

Based on the above conducted numerical studies, an M2RVE model with each lamina consists of 20 fibers (Fig 1b) is created by observing the fibers distribution in a microscopic image of an actual CMC cross-ply laminate. Similar to the UD RVE, the fiber volume fraction in the M2 RVE is maintained at 33%. Elastic and strength properties listed in Table 1 are assigned to the individual constituent materials of the RVE. Moreover, based on the observed microscopic damage pattern in a cross-ply laminate under the applied fiber direction tensile load [4], interlaminar failure is not considered for the current simulations. As shown in Fig 1b, fiber direction tensile load is applied to the M2RVE in the global X-direction.

22

Fig 7a shows the average stress-strain curve obtained from the computational analysis of a cross-ply M²RVE model. As shown in Fig 7b, the initial damage in the laminate is started in the fiber-interphase interface and matrix elements at around 230 MPa stress in the transverse ply of the laminate (perpendicular to the load application direction). Followed by the interface damage and matrix initiation, interphase damage initiates in the same ply at around 365 MPa tensile stress (Fig 7c). As soon as the matrix crack initiates in the 90° ply of the laminate, the matrix damage propagates into the 0° lamina and causes the load drop in the average stress-strain curve (Fig 7a). Loss in load carrying capacity of the considerable volume in the M²RVE triggers the interphase (Fig 7d) and fiber failure (Fig 7e), which leads to the RVE final failure at average stress value of about 505 MPa.

a)

M²RVE under tension - Results for HiPerComp CMC analysis with Tranversely Isotropic Fiber (1.0µm)

Legend:
- EXPERIMENT 0-90
- FEA_M2_EL_CONST_Sm_800_F_CZM_FE_0.4

Axes: True stress, MPa (y-axis); True strain, % (x-axis)

1. Matrix damage
2. Interface damage
3. Interphase damage
4. Fiber failure in the load direction

23
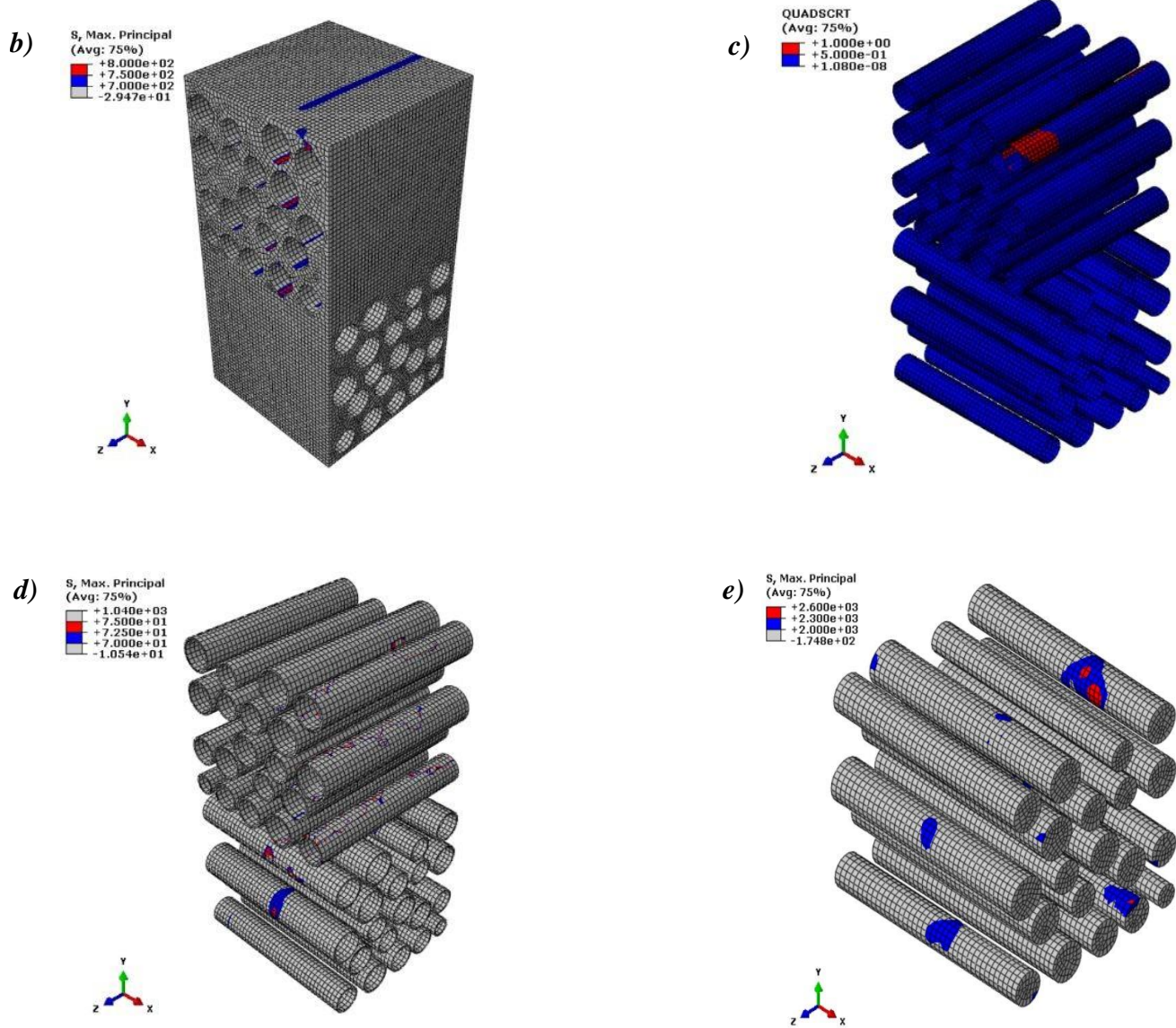
Figure 7 Fiber direction tensile testing of a cross-ply laminate using M2 RVE: a) comparison between experimental [4] and numerical stress-strain curve; b) matrix damage; c) interface damage initiation; d) interphase damage; e) fiber damage

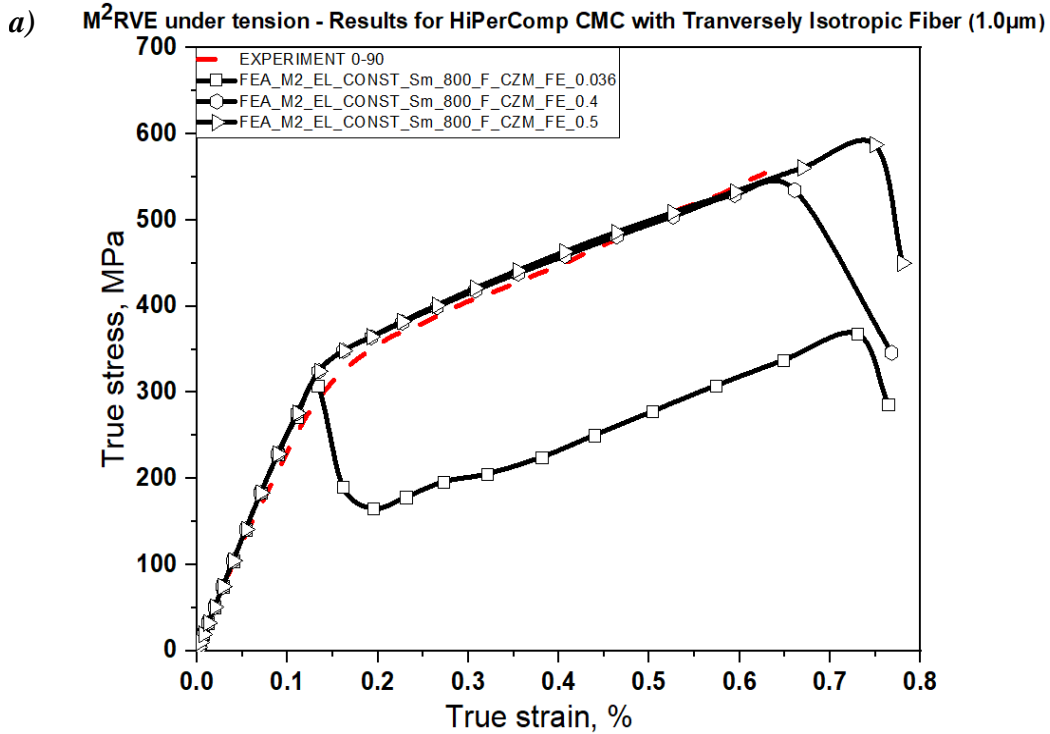### 3.2.1 M²RVE under longitudinal tension – *Effect of RVE size*

Fig 8a compares the predicted average stress-strain curves obtained using RVEs with the varying number of fibers (5 and 10). As illustrated in UD ply above, all these M²RVE are constructed based on the microstructure observed from the microscopic images of an actual 0/90 ply as well. As shown in Fig 8a, *varying the number of fibers does not show any influence in the linear elastic region of the stress-strain curve*. Moreover, the average stress-strain curve predicted using different number of fibers in the M²RVE correlates very well with the experimental stress-strain curve. The observed sequence of damage events in multiple fiber M²RVE's (Fig 7b-e) is similar to that of unidirectional ply. The damage initiates in the matrix and interface simultaneously followed by the damage initiation in interphase and fiber elements. *From the computational studies conducted using different M²RVEs with the varying number of fibers indicate that an M²RVE should contain at least 10 randomly distributed fibers so that the predicted average stress-strain behavior using this volume element is independent of its size and position with the lamina.*
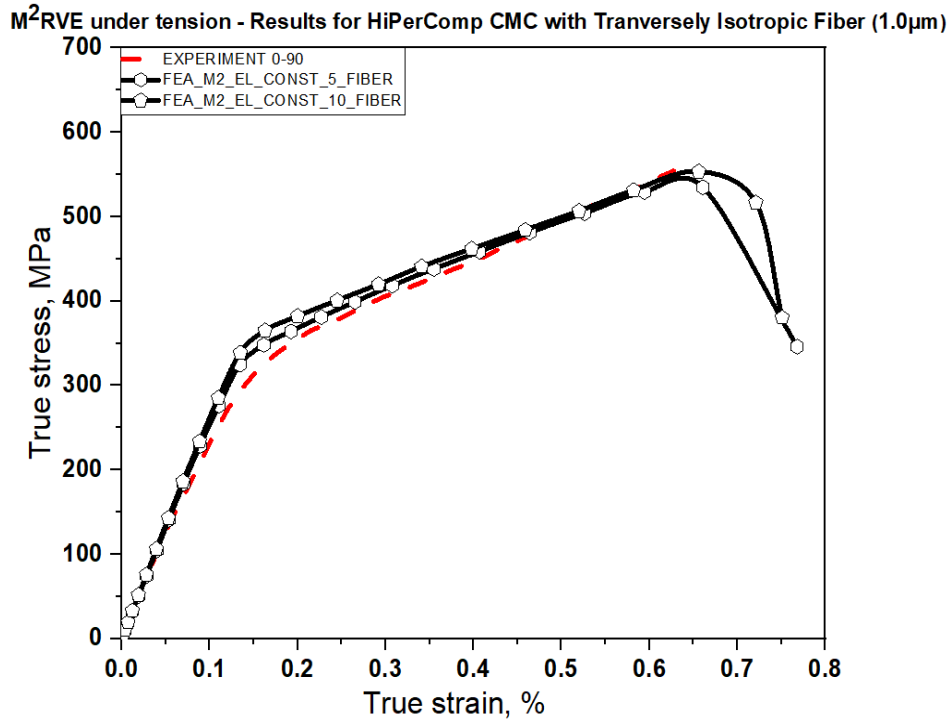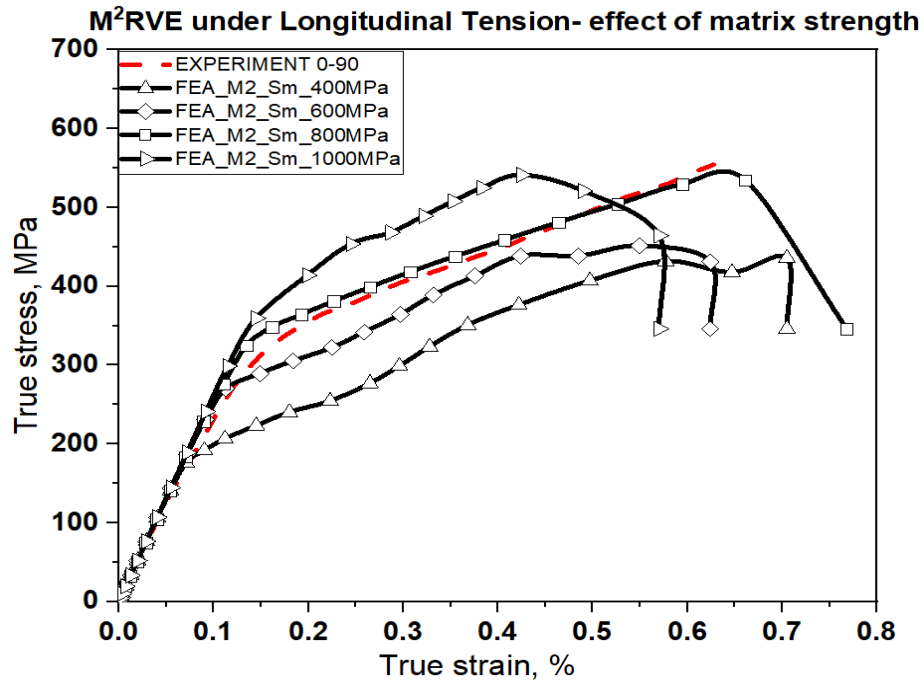

Figure 8 Effect of RVE size on the stress-strain comparison between experimental [4] and numerical stress-strain curve

3.2.2 M²RVE under longitudinal tension – *Effect of matrix material properties*

Analogous to the unidirectional plies, once the *matrix damage initiates* the slope of the stress-strain curve changes considerably (Fig 8a) in 0/90 plies too. Hence, the effect of matrix material properties on the predicted stress-strain behavior of the M²RVE is studied in this section. As was the case in unidirectional plies, here also the matrix (SiC) tensile strength is varied from 400-1000 MPa [18]. The fracture energy of the matrix has been kept constant at 400 J/m2. As shown in Fig 9a, the chosen matrix tensile strength strongly influences the predicted average stress-strain behavior. We observe that for higher strength values, the bend in the graph occurs at higher stress values. The best results are obtained for a matrix strength of 800 MPa. In order to study the effect of matrix fracture energy on the predicted stress-strain behavior, the matrix strength value is kept constant at 800 MPa and the fracture energy value is varied from 36-400 J/m2. As shown in Fig 9b, the slope of the predicted stress-strain curve in the non-linear region is strongly influenced by the chosen fracture energy. *From the current studies, we can conclude that similar to an RVE, the linear elastic stress-strain limit of the M²RVE is controlled by the matrix tensile strength. Whereas the average stress-strain behavior in the non-linear region is controlled by the matrix fracture energy.*

a) **M²RVE under tension - Results for HiPerComp CMC with Tranversely Isotropic Fiber (1.0µm)**

b)

M²RVE under Longitudinal Tension- effect of matrix strength

Figure 9 Effect of matrix material properties on the predicted stress-strain behavior: a) influence of the matrix (SiC) tensile strength; b) influence of matrix fracture energy.

Chapter 4: Conclusions

Detailed micromechanics based finite element analysis methodology is presented to understand the damage initiation and propagation in fiber reinforced CMC (SiC$_f$/BN/SiC) UD lamina and a cross-ply laminate. Detailed RVE modes are generated considering the variation in the fiber diameter as well as the placement of the fibers observed from the microscopic image of an actual CMC lamina and laminate. Brittle cracking criterion is used to model the damage initiation and propagation in the fiber, matrix, and interphase materials. A user material subroutine (VUMAT) is developed and used to perfectly incorporate the matrix damage model. Several State Dependent Variables (SDVs) were included to verify our results with that of Abaqus and study the damage initiation and failure of the materials. Fiber-interphase interface damage is modelled using the cohesive zone modelling approach. Detailed stress-strain and damage analysis under the applied fiber direction tensile loads lead to the following conclusions: i) comparing to the numerical results to the experimental UD composite stress-strain curve, the predicted average stress-strain behavior strongly depends on the RVE size. The generated RVE model should contain at least 15 randomly distributed fibers. Moreover, it should be emphasized here that the RVE size has no influence on the predicted stress-strain behavior in the linear elastic region; ii) In order to obtain satisfactory results in close conformance with the experiments, the generated M^{2}RVE model should contain at least 10 randomly distributed fibers. Moreover, it should be noted here that varying the number of fiber has little influence on the predicted stress-strain behavior of the composite. iii) matrix strength and fracture energy controls the linear elastic limit as well as the stress-strain behavior of the both M^{2}RVE as well as RVE in the post damaged region; iv) from the obtained average stress-strain curve of the RVE and M^{2}RVE, it can be concluded that the matrix damage initiation leads to the localized stress redistribution and triggers the fibers failure. Hence, matrix tensile strength and fracture energy are the key parameters that control the strength and failure strain of the CMC lamina and laminate under applied fiber direction tensile loads, v) the numerical results obtained through the current methodology are consistent with the experimental results and thus, vi) micromechanical analyses can be adequately used to predict the constituents' damage initiation and overall macroscopic stress-strain response of the composite.

References

[1] S. Daggumati, A. Sharma, and Y. S. Pydi, "Micromechanical FE Analysis of SiCf/SiC Composite with BN Interface," *Silicon*, no. https://doi.org/10.1007/s12633-019-00119-3, Feb. 2019.

[2] R. Naslain, "Design, preparation and properties of non-oxide CMCs for application in engines and nuclear reactors: An overview," *Compos. Sci. Technol.*, vol. 64, no. 2, pp. 155–170, 2004.

[3] M. Grujicic, J. S. Snipes, R. Galgalikar, R. Yavari, V. Avuthu, and S. Ramaswami, "Multi-lengthscale derivation of the room-temperature material constitutive model for SiC/SiC ceramic-matrix composites," *Proc. Inst. Mech. Eng. Part L J. Mater. Des. Appl.*, vol. 231, no. 5, pp. 443–462, 2015.

[4] D. G. Dunn, "THE EFFECT OF FIBER VOLUME FRACTION IN HIPERCOMP® SiC-SiC COMPOSITES," ALFRED UNIVERSITY, NEW YORK, 2010.

[5] C. R. W. Evans Anthony Glyn, Rödel J., "Ceramics and ceramic composites as high-temperature structural materials: challenges and opportunities," *Philos. Trans. R. Soc. London. Ser. A Phys.Eng. Sci.*, p. 351.

[6] V. Bheemreddy, K. Chandrashekhara, L. R. Dharani, and G. E. Hilmas, "Computational study of micromechanical damage behavior in continuous fiber-reinforced ceramic composites," *J. Mater. Sci.*, vol. 51, no. 18, pp. 8610–8624, 2016.

[7] A. G. Evans and F. W. Zok, "The physics and mechanics of fibre-reinforced brittle matrix composites," *J. Mater. Sci.*, vol. 29, no. 15, pp. 3857–3896, 1994.

[8] K. M. Sevener, J. M. Tracy, Z. Chen, J. D. Kiser, and S. Daly, "Crack opening behavior in ceramic matrix composites," *J. Am. Ceram. Soc.*, vol. 100, no. 10, pp. 4734–4747, 2017.

[9] J. M. Tracy, "Multi-scale Investigation of Damage Mechanisms in SiC / SiC Ceramic Matrix Composites," University of Michigan, 2014.

[10] B. A. Bednarcyk, S. K. Mital, E. J. Pineda, and S. M. Arnold, "Multiscale modeling of ceramic matrix composites," *56th AIAA/ASCE/AHS/ASC Struct. Struct. Dyn. Mater. Conf.*, no. January, pp.1–8, 2015.

[11] S. Mital, R. Goldberg, and P. Bonacuse, "Modeling of Damage Initiation and Progression in a SiC/SiC Woven Ceramic Matrix Composite," *53rd AIAA/ASME/ASCE/AHS/ASC Struct. Struct. Dyn. Mater. Conf. AIAA/ASME/AHS Adapt. Struct. Conf. AIAA*, no. April, pp. 1–14, 2012.

[12] T. J. Vaughan and C. T. McCarthy, "Micromechanical modelling of the transverse damage behaviour in fibre reinforced composites," *Compos. Sci. Technol.*, vol. 71, no. 3, pp. 388–396, 2011.

[13] C. McCarthy and T. Vaughan, *Micromechanical failure analysis of advanced composite materials*.Elsevier Ltd., 2015.
[14] C. González and J. LLorca, "Mechanical behavior of unidirectional fiber-reinforced polymers under transverse compression: Microscopic mechanisms and modeling," *Compos. Sci. Technol.*,vol. 67, no. 13, pp. 2795–2806, 2007.

[15] L. Yang, Y. Yan, Y. Liu, and Z. Ran, "Microscopic failure mechanisms of fiber-reinforced polymer composites under transverse tension and compression," *Compos. Sci. Technol.*, vol. 72, no. 15, pp. 1818–1825, 2012.

[16] L. Yang, Z. Wu, Y. Cao, and Y. Yan, "Micromechanical modelling and simulation of unidirectional fibre-reinforced composite under shear loading," *J. Reinf. Plast. Compos.*, vol. 34, no. 1, pp. 72–83, 2015.

[17] M. Romanowicz, "A numerical approach for predicting the failure locus of fiber reinforced composites under combined transverse compression and axial tension," *Comput. Mater. Sci.*, vol.51, no. 1, pp. 7–12, 2012.

[18] M. Braginsky and C. P. Przybyla, "Simulation of crack propagation/deflection in ceramic matrix continuous fiber reinforced composites with weak interphase via the extended finite element method," *Compos. Struct.*, vol. 136, pp. 538–545, 2016.

[19] S. K. Mital, B. A. Bednarcyk, S. M. Arnold, and J. Lang, "Modeling of Melt-Infiltrated SiC/SiC
Composite Properties October 2009," no. October 2009, 2009.

[20] A. . Fallis, "Micromechanical," *J. Chem. Inf. Model.*, vol. 53, no. 9, pp. 1689–1699, 2013.

[21] C. Chateau, L. Gélébart, M. Bornert, and J. Crépin, "Micromechanical modeling of the elastic behavior of unidirectional CVI SiC/SiC composites," *Int. J. Solids Struct.*, vol. 58, pp. 322–334, 2015.

[22] E. Totry, C. González, and J. LLorca, "Prediction of the failure locus of C/PEEK composites under transverse compression and longitudinal shear through computational micromechanics,"
Compos. Sci. Technol., vol. 68, no. 15–16, pp. 3128–3136, 2008.

[23] D. Garoz *et al.*, "Consistent application of periodic boundary conditions in implicit and explicit finite element simulations of damage in composites," *Compos. Part B*, vol. 168, no. December 2018, pp. 254–266, 2019.

[24] "ABAQUS (2010) Analysis User's Manual. Version 6.10," *Dassault Systemes Simulia, Inc*.

[25] J. G. Rots, "COMPUTATIONAL MODELING OF CONCRETE FRACTURE," *Diss. Delft Univ.Technol,* p. 0, 1988.

[26] A. Hillerborg, M. Modéer, and P. E. Petersson, "Analysis of crack formation and crack growth in concrete by means of fracture mechanics and finite elements," *Cem. Concr. Res.*, vol. 6, no. 6, pp.773–781, 1976.

[27] Z. P. Bazant and B. H. Oh, "Crack band theory for fracture of concrete," *Matériaux Constr.*, vol.16, no. 3, pp. 155–177, 1983.

[28] J. G. Rots and J. Blaauwendraad, "Crack models for concrete: discrete or smeared? Fixed multidirectional or rotatin?," *Heron*, vol. 34, no. 1, pp. 3–59, 1989.

[29] A. G. Evans, J. -M Domergue, and E. Vagaggini, "Methodology for Relating the Tensile Constitutive Behavior of Ceramic-Matrix Composites to Constituent Properties," *J. Am. Ceram. Soc.*, vol. 77, no. 6, pp. 1425–1435, 1994.

[30] J. A. CQPPOLA and R. C. BRADT, "Measurement of Fracture Surface Energy of SiC," *J. Am.Ceram. Soc.*, no. September, pp. 455–460, 1972.